Materials Horizons

ROYAL SOCIETY OF CHEMISTRY

COMMUNICATION

View Article Online
View Journal | View Issue

Check for updates

Cite this: *Mater. Horiz.*, 2024, 11, 2388

Received 20th November 2023,
Accepted 27th February 2024

DOI: 10.1039/d3mh01966g

rsc.li/materials-horizons

Robust multiferroicity and magnetic modulation of the ferroelectric imprint field in heterostructures comprising epitaxial $Hf_{0.5}Zr_{0.5}O_2$ and Co†

Tetiana Zakusylo,[a] Alberto Quintana,[a] Veniero Lenzi,[b] José P. B. Silva,[cd] Luís Marques,[cd] José Luís Ortolá Yano,[a] Jike Lyu,[a] Jordi Sort,[ef] Florencio Sánchez *[a] and Ignasi Fina *[a]

Magnetoelectric multiferroics, either single-phase or composites comprising ferroelectric/ferromagnetic coupled films, are promising candidates for energy efficient memory computing. However, most of the multiferroic magnetoelectric systems studied so far are based on materials that are not compatible with industrial processes. Doped hafnia is emerging as one of the few CMOS-compatible ferroelectric materials. Thus, it is highly relevant to study the integration of ferroelectric hafnia into multiferroic systems. In particular, ferroelectricity in hafnia, and the eventual magnetoelectric coupling when ferromagnetic layers are grown atop of it, are very much dependent on quality of interfaces. Since magnetic metals frequently exhibit noticeable reactivity when grown onto oxides, it is expected that ferroelectricity and magnetoelectricity might be reduced in multiferroic hafnia-based structures. In this article, we present excellent ferroelectric endurance and retention in epitaxial $Hf_{0.5}Zr_{0.5}O_2$ films grown on buffered silicon using Co as the top electrode. The crucial influence of a thin Pt capping layer grown on top of Co on the ferroelectric functional characteristics is revealed by contrasting the utilization of Pt-capped Co, non-capped Co and Pt. Magnetic control of the imprint electric field (up to 40% modulation) is achieved in Pt-capped Co/$Hf_{0.5}Zr_{0.5}O_2$ structures, although this does not lead to appreciable tuning of the ferroelectric polarization, as a result of its high stability. Computation of piezoelectric and flexoelectric strain-mediated mechanisms of the observed magnetoelectric coupling reveal that flexoelectric contributions are likely to be at the origin of the large imprint electric field variation.

New concepts

Multiferroic structures based on epitaxial ferroelectric hafnia prepared on silicon are newly developed and evaluated for their integration into magnetoelectric devices. So far, all reported hafnia-based multiferroic structures exhibit a polycrystalline character, precluding a full understanding of their magnetoelectric performance due to the presence of grains with several orientations, defects and blurry interfaces. The characterization of epitaxial ferroelectric hafnia structures combined with ferromagnetic cobalt films, analyzed in this work, allows to disclose the relevant role of the magnetic material reactivity on the robustness of ferroelectricity and the whole structure. Here we provide the first evidence of direct magnetoelectric effects in a multiferroic system based on epitaxial hafnia, where magnetic and ferroelectric properties are highly robust. In spite of growing this system on a rigid substrate (with the concomitant clamping effects) our work reveals the existence of a magnetically-induced additional imprint electric field, whose origin is ascribed to flexoelectric (*i.e.*, strain gradient-mediated) effects.

Introduction

Ferroelectric hafnia is attracting the interest of the scientific community and industry due to its CMOS compatibility, which makes it appealing for non-volatile memory applications.[1–3] Doped HfO_2 is ferroelectric as a result of the stabilization of the metastable orthorhombic phase in thin film form. The robustness of the ferroelectric character of doped HfO_2 is highly

[a] *Institut de Ciència de Materials de Barcelona (ICMAB-CSIC), Campus UAB, Bellaterra 08193, Barcelona, Spain. E-mail: fsanchez@icmab.es, ifina@icmab.es*
[b] *CICECO – Aveiro Institute of Materials, Department of Chemistry, University of Aveiro, Aveiro 3810-193, Portugal*
[c] *Physics Center of Minho and Porto Universities (CF-UM-UP), University of Minho, Campus de Gualtar, Braga 4710-057, Portugal*
[d] *Laboratory of Physics for Materials and Emergent Technologies, LapMET, University of Minho, Braga 4710-057, Portugal*
[e] *Departament de Física, Universitat Autònoma de Barcelona, Bellaterra 08193, Spain*
[f] *ICREA, Pg. Lluís Companys 23, Barcelona 08010, Spain*

† Electronic supplementary information (ESI) available. See DOI: https://doi.org/10.1039/d3mh01966g

dependent on the type of dopant and the doping level.[4,5] Up to now, 50% Zr doping (HZO) has been demonstrated to be the optimal composition to attain large polarization values combined with good endurance/retention performance.[6] Interestingly, ferroelectricity has been also found to depend on the electrode selection, even when ideal doping conditions are used,[7–13] thus revealing a significant influence of the films' interfaces on the device functional properties.

Multiferroic magnetoelectric materials, which combine ferroelectric and ferromagnetic/antiferromagnetic orders with a mutual coupling between them, are of large technological interest since they allow writing of magnetic data directly using voltage instead of electric current (or magnetic fields), thus minimizing Joule heating effects.[14] Recently, energy-efficient computing operations achieving large reduction in power consumption have been demonstrated through the use of multiferroic $BiFeO_3$.[15] However, $BiFeO_3$ (and most other single-phase multiferroics) are not CMOS compatible and, thus, their device integration is far from obvious.[16]

Contrary to single-phase multiferroics, composite multiferroic materials could circumvent CMOS compatibility problem since they are based on combinations of ferroelectric and ferromagnetic materials where coexistence of electric and magnetic orders is not required in each of the components individually. Instead, the two orders can exist in two separate coupled films, thus widening the range of materials that can be employed and offering more options for their integration into devices (*i.e.*, increasing the overall device viability).[17,18]

In composite multiferroic materials the electric control of magnetization, so-called 'converse magnetoelectric coupling', can originate from several mechanisms that have been studied extensively in the literature.[19–21] These mechanisms can be summarized as: (i) modulation of carrier density by electric-field effect; (ii) modification of the magnetic anisotropy by changing the hierarchy of the electronic orbitals and their electronic filling also by electric field; and (iii) modulation magnetic properties by strain coupling between piezoelectricity and magnetostriction of the ferroelectric and ferromagnetic materials respectively.[19–21] Alternatively, magneto-ionic effects may also lead to changes of magnetization under voltage.[22] 'Direct magnetoelectric coupling', *i.e.* magnetic control of the ferroelectric polarization, has been much less investigated,[16,23] in spite of being also highly interesting for relevant applications.[24] The possible origin of direct magnetoelectric coupling is limited to fewer mechanisms, thus simplifying its understanding. In general, direct magnetoelectric effects originate from strain-mediated coupling. This type of coupling usually presents the inconvenient of the substrate-clamping effects when magnetoelectric systems are grown onto rigid substrates.[25,26] In this regard, strategies have been developed to partially avoid substrate-clamping negative impact, like the use of flexible (instead of rigid) materials, or others.[27–29]

Irrespectively of whether direct or converse magnetoelectric responses are characterized, most multiferroic composite materials are based on complex oxides. Because of the difficulty of integrating these oxides into CMOS technology without drastically lowering their performance, the potential use of these materials in applications is still limited. Instead, ferroelectric hafnia-based multiferroics are more attractive due to their CMOS compatibility. However, the investigation of magnetoelectric coupling in ferroelectric hafnia-based systems is incipient. Dmitryeva *et al.*[30] reported that in HZO/Ni based structures, redox reactions at the interface can be at the origin of the observed changes in the electronic configuration of Ni. Vermeulen *et al.* found evidences of changes of the magnetization of CoPt on Al:HfO_2 upon ferroelectric switching.[31] In these two cases, the ferroelectric properties (*e.g.*, the relatively low obtained polarization values, of about 6 and 7 μC cm^{-2}, respectively), are influenced by the annealing required to stabilize the ferroelectric phase. This annealing results in a degradation of the interface between the ferroelectric oxide and the highly reactive ferromagnetic metal grown on top of it. Lancaster *et al.*[32] reported state-of-the-art ferroelectric properties in $Hf_{0.5}Zr_{0.5}O_2$ adjacent to a graphene/Co/heavy metal stack. Large polarization values were only obtained while using an interface oxide layer, likely at the expenses of the magnetoelectric coupling. Epitaxial films on perovskite substrates do not require of post-annealing to attain good ferroelectric properties,[33,34] allowing to produce sharper interfaces compared with polycrystalline films. This facilitates the basic understanding of the induced effects while eventually helping to improve the strength of the magnetoelectric coupling. The suitability of epitaxial hafnia films for their integration into multiferroic devices has been demonstrated in HZO tunnel junctions using Co top electrodes.[35,36] However, the ultrathin character of the tunnel barriers with the concomitant expected decrease of polarization and the reported significant presence of ionic effects might hinder genuine magnetoelectric coupling.

From the above examples, it is clear that ferroelectric properties of hafnia can be largely affected by interfaces. The reactivity of magnetic metals poses a challenge to obtain multiferroic devices with robust ferroelectric and ferromagnetic properties and simultaneously large magnetoelectric coupling. In the present work, we study in detail the ferroelectric properties of epitaxial HZO films grown on silicon, while using Co and Pt layers as top electrodes. The polarization values and retention are found to be large in all the studied cases. In turn, endurance is found to be highly depending on whether a Pt capping layer is grown onto the Co electrode. We report that uncapped Co electrodes show very bad endurance properties and Pt-capped Co electrodes show a remarkable endurance, comparable to that of Pt electrodes. Direct magnetoelectric experiments reveal the occurrence of an imprint electric field that changes in strength upon the application of a magnetic fields, whereas the remanent polarization remains insensitive. Density functional theory (DFT) and analytical calculations reveal the origin of the observed magnetoelectric coupling.

Materials and methods

An epitaxial 9.6 nm-thick $Hf_{0.5}Zr_{0.5}O_2$ film was grown on a $La_{2/3}Sr_{1/3}MnO_3$ (LSMO) bottom electrode by pulsed laser deposition

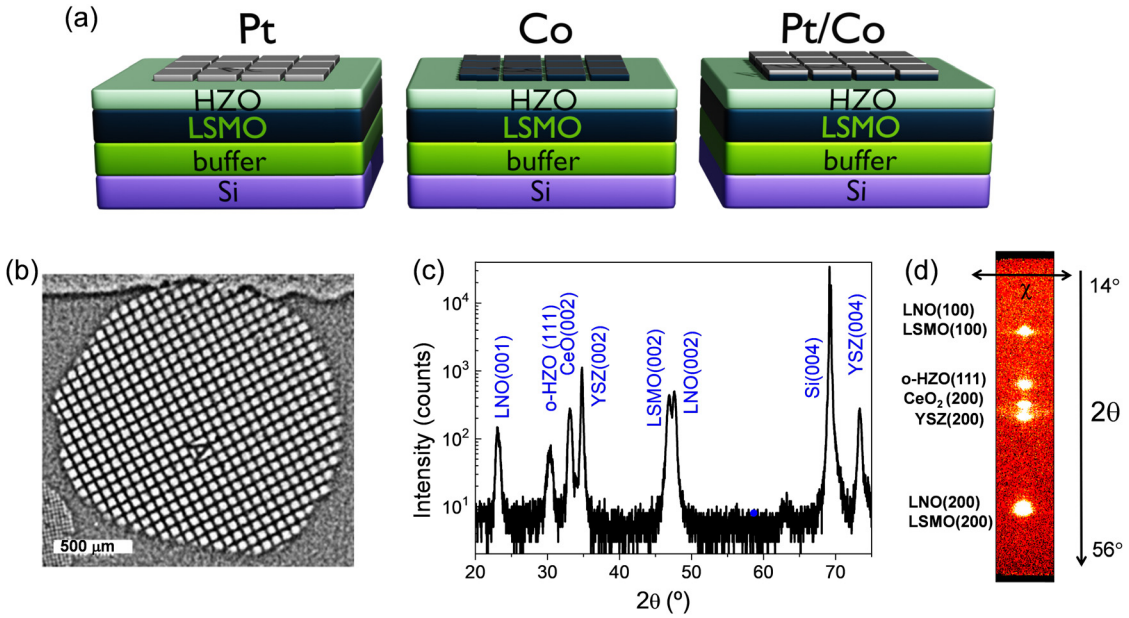

Fig. 1 (a) Sketch of the characterized structures. Pt, Co and Co capped with Pt electrodes are deposited on the HZO film previously grown on buffered Silicon. (b) Top-view image of the electrodes. (c) XRD θ–2θ scan of the deposited films prior to the growth of the top electrodes. (d) XRD 2θ–χ frame.

(PLD). Both layers were grown sequentially on top of buffered Si. The buffer layer was a $LaNiO_3/CeO_2/YSZ$ stack. The CeO_2–$LaNiO_3$ layers are deposited to reduce the lattice mismatch between LSMO and YSZ to ensure epitaxial growth of LSMO. The whole heterostructure was fabricated in a single process by PLD. The deposition conditions for each layer are summarized elsewhere.[37] The top 60 μm × 60 μm electrodes [Pt (20 nm), Co (20 nm), Pt/Co (20/3 nm, being Pt the top capping layer)] were deposited *ex situ* on top of the aforementioned heterostructures by DC magnetron sputtering using a shadow mask. The actual contact areas of the top electrodes were measured using optical microscopy images. The resulting multilayer structures are schematized in Fig. 1(a) and an image of the top electrode array is shown in Fig. 1(b).

The crystal structure was characterized by X-ray diffraction (XRD) using Cu K_α radiation. θ–2θ scans were measured using a Siemens D5000 diffractometer equipped with a point detector and using a Bruker D8-ADVANCE diffractometer equipped with a two-dimensional (2D) detector. X-ray photoelectron spectroscopy (XPS) was performed in ultrahigh vacuum of 5×10^{-10} mbar with a SPECS Phoibos 150 hemispherical analyzer using monochromatic Al Kα radiation with an energy of 1486.6 eV. Samples were in contact with air when transferred from the PLD chamber to the UHV XPS chamber. Electric characterization of the samples was performed using TFAnalyser 2000 system, which permits performing polarization hysteresis loops, retention, and fatigue measurements. Ferroelectric loops and endurance were measured using dielectric leakage current compensation and retention data through the positive up negative down (PUND) method.[38,39] The endurance measurements were performed up to 10^8 cycles, at 100 kHz and using voltage bipolar pulses of 4 V. Retention was measured using 5 V saturation voltage up to 10^3 s. Leakage current has been measured using 1 s integration time with the same platform. Electric characterization under magnetic field was performed using Lakeshore EMPX-HF system. Magnetocapacitance measurements have been performed at 100 kHz with an excitation voltage of 300 mV using an Agilent 4192A LF impedance analyzer. All the measurements were done electrically biasing the top electrode and grounding the bottom electrode using silver paste.

All DFT calculations have been performed using VASP,[40,41] taking the PBEsol[42] functional. While core states were treated within the projector augmented wave framework,[43] the following states were considered explicitly: 2s2p for O, 4s4p5s4d for Zr and 5s5p6s5d for Hf. A (111)-oriented 144-atoms HZO special quasirandom structure (SQS)[44] was considered, and we adopted a Gamma-centered 2 × 2 × 3 *k*-point grid and a plane wave energy cutoff of 600 eV. The stress-free structure was relaxed with a strict force threshold of 0.1 meV $Å^{-1}$ and a pressure threshold of 0.1 GPa. Equibiaxial strain conditions were applied to the in-plane lattice parameters *a* and *b* while the out-of-plane parameter *c* was allowed to freely relax, along with all the atomic positions. In strained systems force and pressure (along *c*) thresholds were 1 meV per atom and 0.1 GPa respectively. The modern theory of polarization was used to obtain the polarization values.[45] The piezoelectric tensor was calculated for the stress-free HZO using a density functional perturbation theory approach to obtain the electronic contribution[46] and a finite differences method (with atomic displacements of 0.015 Å) to evaluate the ionic contribution.

Results

The XRD characterization, shown in Fig. 1(c) and (d), reveals diffraction peaks from the different underlayers (buffer and

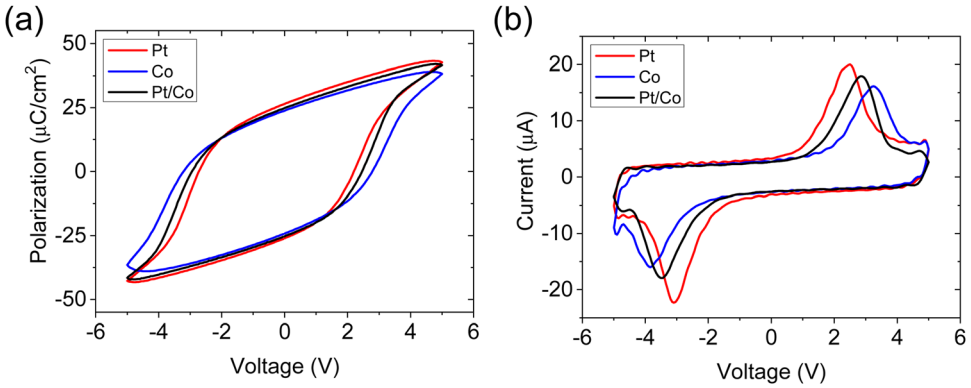

Fig. 2 (a) and (b) Ferroelectric *P*–*V* and *I*–*V* polarization loops, respectively, obtained in capacitor configuration with Pt, Co and Pt/Co top electrodes.

LSMO electrode), together the (111) peak from the orthorhombic HfO_2 phase. The *P*–*E* loops and corresponding *I*–*V* curves for the samples with Pt, Co and Pt/Co top electrodes are shown in Fig. 2(a) and (b), respectively. Similar P_r values are obtained for all cases, being slightly lower for Co and Pt/Co (23.8 and 25.0 μC cm^{-2}, respectively, in front of 26.5 μC cm^{-2} for Pt). E_c is slightly larger for Co and Pt/Co (3.1 and 2.8 MV cm^{-1}), respectively, in front of Pt (2.4 MV cm^{-1}). The imprint electric field is negative, thus favoring downwards polarization, *i.e.*, oriented towards the bottom LSMO. E_{imp} values are −260, −210 and −205 kV cm^{-1} for samples with Pt, Co and Pt/Co top electrodes, respectively.

Endurance and retention characterizations are shown in Fig. 3. By comparing Fig. 3(a)–(c), it can be observed that the

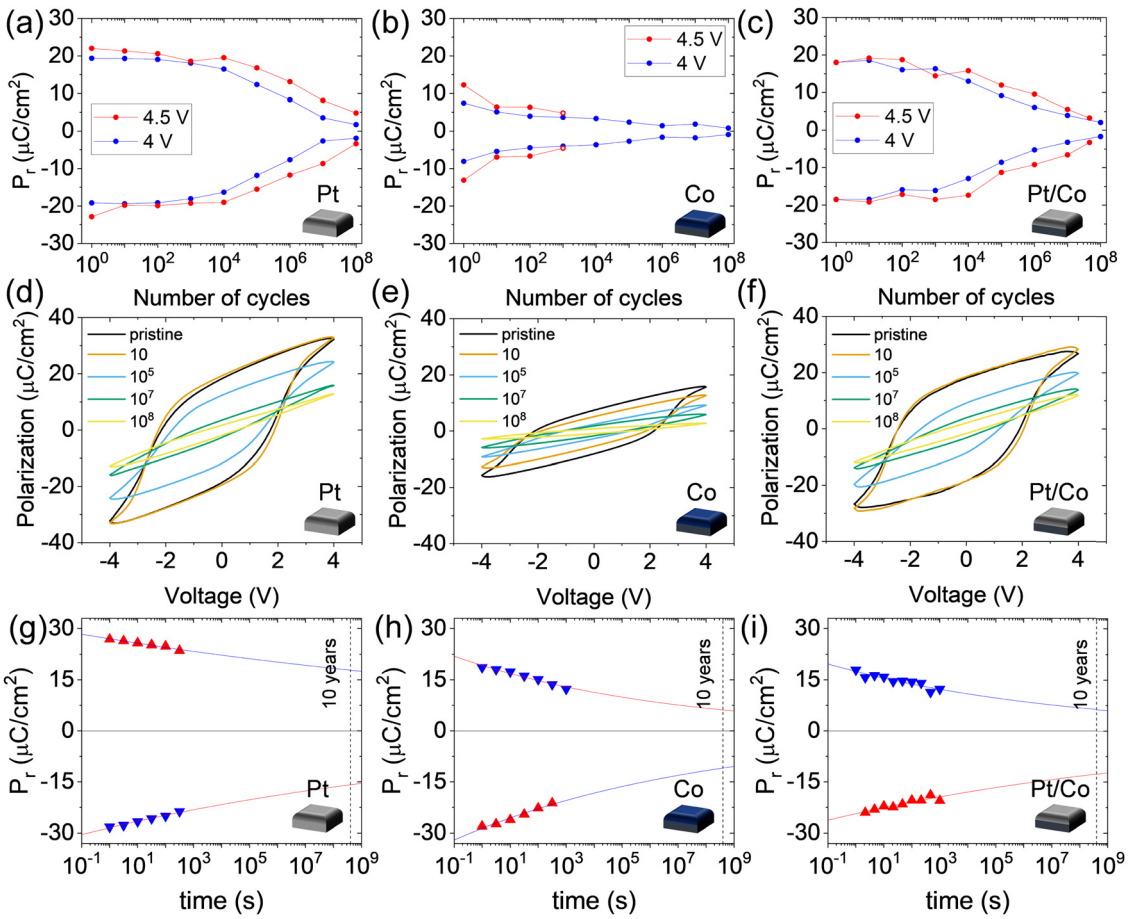

Fig. 3 (a)–(c) Endurance, measured with bipolar rectangular pulses of frequency 100 kHz and amplitude of indicated voltage using Pt, Co and Pt/Co top electrodes, respectively. (d)–(f) *P*–*V* loops measured after the indicated number of cycles using Pt, Co and Pt/Co top electrodes, respectively. (g)–(i) Retention of the samples using Pt, Co and Pt/Co top electrodes, respectively.

endurance is worse for the sample with Co electrode, being the one with Pt the best performing. Note that 4 V has been used in all endurance tests, which results in not fully saturated polarization while cycling, especially for the Co case due to its larger E_c. Even considering that polarization has not been saturated, the endurance is worse when using Co. The poor robustness of the film with Co compared to that with Pt top electrode can be ascribed to the known impact of the use of reactive top electrodes on the endurance properties, due to the migration of oxygen vacancies through the interface or formation of other defects.[7] Leakage current measurements (see ESI†) indicate larger leakage in samples with Co in front of those with Pt, reinforcing the expected presence of more defects if Co is present. However, XRD characterization when using different electrodes does not reveal any change on the orthorhombic (111) diffraction peak (see ESI†). XPS characterization in nominally equal samples reveal that, whereas changes on the Hf oxidation state cannot be observed, changes are indeed present when comparing the XPS spectra of Co in the Co and Pt/Co cases, being Co more oxidized in absence of Pt. Therefore, it can be concluded that Co is in fact more oxidized, confirming its larger reactivity if not capped with Pt (see ESI†). Fig. 3(d)–(f) show the ferroelectric loops collected after the indicated number of cycles. A similar good performance for top Pt and Pt/Co electrodes, compared with Co, is observed. Retention characterization [Fig. 3(g)–(i)] shows that stability of polarization for the Pt case is the largest. The use of Pt/Co electrodes results in slightly better retention than for Co. In any case, the extrapolated to 10 years 2^*P_r is, in all cases, above 15 μC cm^{-2}. Note that polarization values are slightly lower in the retention tests compared with results presented in Fig. 2 due to combined presence of small fluid imprint field contribution, resulting in underestimation of read polarization, and polarization back-switching at <1 s.[47]

MOKE magnetic loops measured under in-plane applied magnetic field for the different used top electrodes are shown in Fig. 4(a). It can be observed that hysteresis is present in all cases except for Pt due to its non-magnetic nature. The absence of ferromagnetic response for the sample with Pt also indicates that the contribution from the magnetic bottom electrode, LSMO, is not detectable by MOKE. The sample containing Pt/Co shows a coercive field of 80 Oe, while that with Co shows a significantly larger coercive field, *i.e.*, 240 Oe. This can be ascribed to the larger presence of cobalt oxide in this case, which increases the number of defects and reduces the effective Co thickness, both resulting in an increase of the magnetic coercive field.[48] The presence of exchange bias effects between cobalt and cobalt oxide could also contribute to the larger magnetic coercive field, although the Néel temperature of CoO is just around room temperature.[49] The collected ferroelectric and magnetic properties are summarized in Fig. 4(b). It can be observed that, whereas the polarization values are similar in all the samples, retention is good for Co and Pt/Co but that for Pt is even better. When using Co, only Pt/Co top electrodes show endurance similar to Pt. Interestingly, E_{imp} in lower when using Co compared to the sample with Pt top electrode, which can be ascribed to the lower workfunction of Co in front of Pt. Note that the presence of cobalt oxide should not affect band bending slope due to its insulating character. Ferromagnetic response is only found when incorporating a top electrode that contains Co.

Finally, we turn on the possible presence of direct magnetoelectric coupling. Fig. 5(a) and (b) show the *I*–*V* and the corresponding *P*–*V* loops of the Pt/Co/HZO/LSMO structure while sequentially turning "on" and "off" an in-plane magnetic field of 6 kOe, which is well-above the magnetic coercive field of any of the investigated samples. Some interesting small effects are found. A zoom of the current switching peak at positive voltages is shown in Fig. 5(c). It can be observed that peak position shifts to lower voltages under the application of magnetic field. The coercive electric field, E_c, for positive and negative voltages is plotted in Fig. 5(d) as a function of sequentially "on"/"off" applied magnetic field [as indicated in the bottom panel in Fig. 5(d)]. The data reveal that the negative voltage E_c variation is negligible. However, for positive voltage E_c decreases when magnetic field is applied. In addition, E_c tends to slightly decrease with step number due to a small fatigue contribution. A systematic variation of E_{imp} is also observed, being it ≈40% more negative under the application of magnetic field. This systematic variation is not observed when Pt is used as the top electrode (see ESI†). Finally, the P_r values (left-axis) do not show a clear significant variation under

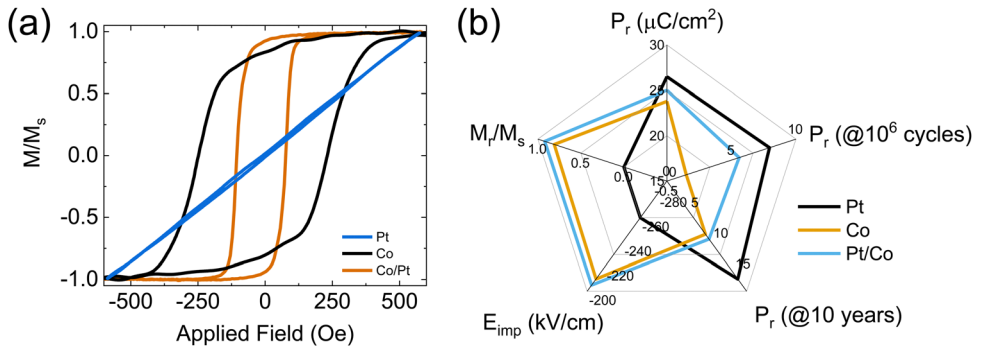

Fig. 4 (a) MOKE signal normalized to its value at 550 Oe when using Pt, Co and Pt/Co top electrodes. (b) Summary of ferroelectric and magnetic characteristic parameters of samples with Pt, Co and Pt/Co top electrodes.

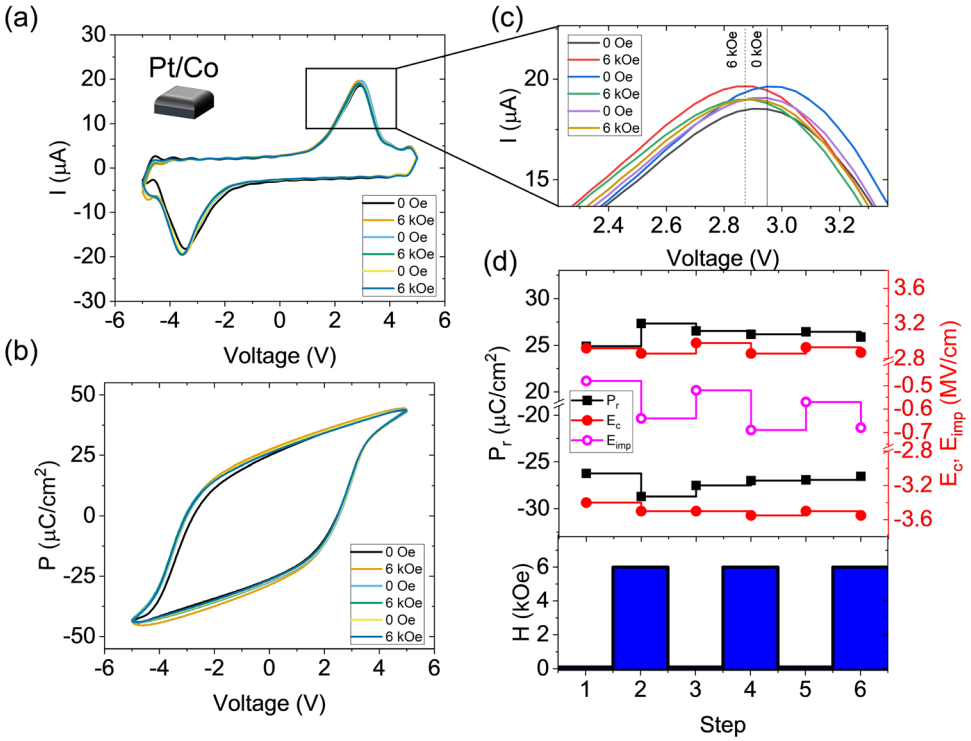

Fig. 5 (a) I–V loops measured under 0 and 6 kOe, sequentially. (b) Zoom of (a) near the positive switching peak position. (c) P–V loops measured under 0 and 6 kOe, sequentially. (d) P_r, E_c and E_{imp} values extracted from loops collected at 0 and 6 kOe recorded sequentially. Note that in the top graph of panel (d), the y-axis (left and right) are truncated.

application of magnetic field. Careful inspection allows to see that P_r only shows a variation between the first and second loop, and a slight decreasing trend upon successive cycling, again resulting from fatigue. The null variation of polarizability under magnetic field has been confirmed by magnetodielectric measurements, where constant capacitance upon magnetic field application has been found (see ESI†).

Discussion

Interesting phenomenological effects can be derived from the results described above. First, magnetoelectric coupling is not seen in the sample with a top Pt electrode, thus disregarding any relevant role from the bottom LSMO electrode on magnetoelectricity (see ESI†). This result is expected since LSMO is likely to be more clamped by the substrate than the top Co electrode. In turn, the E_c increase due to a series resistance effect could be an extrinsic mechanism resulting in magnetoelectric effects. It is also known that interface capacitance (due to, for instance, band bending at the metal/ferroelectric interface) can result in the presence of Maxwell–Wagner effects. Maxwell–Wagner resonance can lead to large extrinsic direct magnetodielectric effects, ultimately resulting from the presence of magnetoresistance.[50] However, magnetoresistance effects would be expected to produce a symmetric variation of E_c and no variation of E_{imp} (see ESI†). Additionally, Co magnetic state is unlikely to produce any magnetoelectric coupling mediated by band bending modulation because work function (Fermi level position in semiconductors) is not sensitive to magnetic field. Therefore, these extrinsic effects are also disregarded. Conversely, the mechanical coupling between the Co and HZO layers can be an intrinsic mechanism at the origin of the observed magnetoelectric effect. Therefore, the role of the piezoelectric effect has been investigated. We have calculated, using density functional theory, the change of polarization ΔP_s under compressive or tensile equibiaxial in-plane strain in the 2% range (Fig. 6(a)). While the ΔP_s could be above 10% for the larger compressive/tensile strain values considered, small changes are obtained for the small strains values expected in our system. By performing further calculations for strains in the range $\pm 0.01\%$ (Fig. 6(b)), we observed that the ΔP_s is minute (0.08%).

To further elucidate the role of the piezoelectric effect in the observed polarization changes, we calculated the piezoelectric tensor of (111)-oriented HZO, as shown in Table 1. By considering an in-plane equibiaxial strain in the 0.0005% range, consistent with the strain induced by the Co magnetostriction ($\lambda \cong -5 \times 10^{-6}$), we calculated an induced ΔP_s of about 0.003%, much below the noise level of the experimental set-up. Therefore, despite piezoelectric effects can be important at larger strains, their impact on ferroelectric polarization in the very small strain range explored here is not remarkable, which is in agreement with the experimental observations.

In any case, a decrease of polarization or coercive field as a result of only piezoelectric effects should result in a symmetric

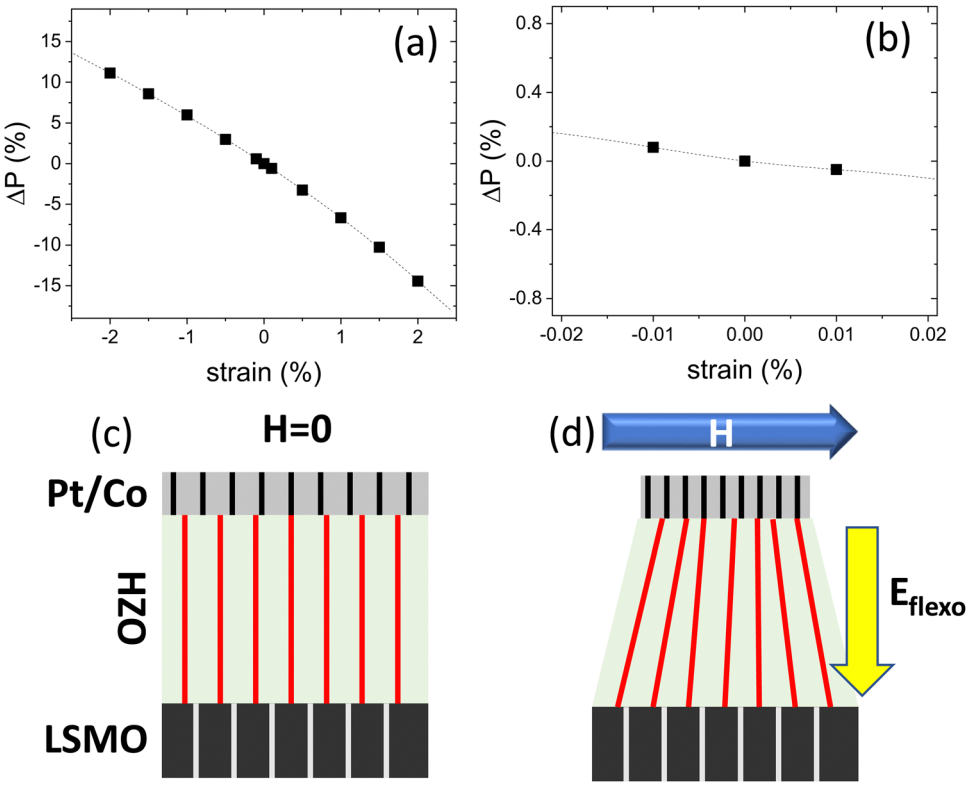

Fig. 6 (a) Density functional theory calculations of the change in polarization along the (111) direction as a function of applied equibiaxial in-plane strain for (111)-oriented HZO. (b) Idem for larger strain values. Sketch of the HZO deformation under compressive strain generated by the Co layer (c) without application of magnetic field and (d) with the application of magnetic field.

Table 1 Piezoelectric tensor $e_{\alpha i}$ of HZO, in μC cm^{-2}, where α is a Cartesian component and i is a strain component in the Voigt notation. Since the tensor was calculated for a (111)-oriented cell, the z axis corresponds to the (111) direction

	xx	yy	zz	xy	xz	yz
x	75.647	136.567	159.633	−0.936	0.663	−26.479
y	89.008	59.78	27.541	10.046	7.372	6.918
z	−130.972	−63.014	−66.366	8.866	4.061	−20.592

variation of positive and negative remanent polarization and coercive fields. From data included in Fig. 5(d), one cannot infer systematic symmetric changes for $\pm P_r$ or $\pm E_c$. Thus, we can further conclude that relevant piezoelectric effect on the system do not have a sizeable impact on the ferroelectric properties of hafnia, indicating possible contribution of flexoelectric effects.

Since Co magnetostriction is negative, upon application of magnetic field the flexoelectric electric field is expected to point downwards (negative sign),[51] thus increasing the negative imprint electric field under magnetic field, as experimentally observed (see schematics in Fig. 6(c) and (d)). Due to the challenging computation of flexoelectric effects, the electric field associated to the induced flexoelectric effect (E_{flexo}) has been obtained using the following analytical expression:[52–54] The electric field associated to the induced flexoelectric effect (E_{flexo}) can be computed as follows:[52–54]

$$E_{flexo} = \delta \frac{e}{\varepsilon_0 a} \frac{\partial u}{\partial x}$$

where E_{flexo} is the electric field induced by magnetic field, δ is a scaling factor, e is the electronic charge, a is the lattice constant along the electric field direction (here d_{111} = 2.948 Å), $\frac{\partial u}{\partial x}$ is the additional strain induced by magnetic field and ε_0 is the permittivity of free space. If we assume that HZO is fully clamped to LSMO and the latter does not play any role, $\frac{\partial u}{\partial x}$ is here equal to magnetostriction ($\lambda \cong -5 \times 10^{-6}$)[51] divided by the film thickness. The quantification of flexoelectric coefficient in ferroelectric HfO_2 is inexistent. Therefore, if we assume δ = 1–10 (as in other studied ferroelectric perovskites),[55] a flexoelectric additional imprint field of −10 kV cm^{-1} is obtained, which is far from the near −0.1 MV cm^{-1} experimentally observed but of the same order and sign. Depending on the Co microstructure, the picture can become more complex due to the high interdependence between λ and microstructure. Also note that it should be taken into account that when an in-plane magnetic field is applied, Co should expand along the perpendicular-to-film direction. It has also been reported that magnetic order and ionic effects can be coupled.[56,57] Besides this, recent results show that intertwined contributions of ionic

and ferroelectric effects can be present in ferroelectric hafnia.[58–60] Therefore, complex additional coupling mechanisms might exist. All in all, mechanical coupling can partially explain the observed effects, although full determination of the ultimate underlying mechanism would require additional characterizations in systems showing larger effects.

We would like to also point out the small impact of the E_{imp} variation on the measured P_r. This can be ascribed to the fact that $E_{imp} \ll E_c$. Thus, only variations of E_{imp} in the order of 1 MV cm^{-1} can be expected to cause a sizeable change of polarization. In this regard, the study of systems based on La:HfO_2[61] or others, where ferroelectric coercivity has been found to be lower, can be of interest for improved direct magnetoelectric effects.

Conclusions

Pt/Co/HZO/LSMO is shown to be a robust multiferroic heterostructure with remarkable combination of high polarization-endurance-retention. The relevant role of the Pt capping on the ferroelectric properties has been revealed, which indicates that high materials quality is required to reduce chemical intermixing that can hinder genuine properties when magnetic materials are used as electrodes. The Pt/Co/HZO structure has been used to evaluate the direct magnetoelectric coupling, so far never reported in hafnia-based multiferroic systems. A 40% variation of E_{imp} is found, which is ascribed to strain-mediated coupling with participation of flexoelectric effects. The E_{imp} variation has no impact on the measured polarization, which remains stable thanks to the high coercive ferroelectric field of hafnia. This agrees well with the small expected changes on polarization according to DFT calculations, which show that despite the piezoelectric contribution on the mechanical coupling can be relevant, it does not result in sizeable effects in the case of small strains regime. Overall, this work constitutes a leap for the understanding of magnetoelectric phenomenology in multiferroic systems based on hafnia, opening the possibility for new functionalities and devices utilizing CMOS-compatible ferroelectric materials.

Conflicts of interest

There are no conflicts to declare.

Acknowledgements

Financial support from the Spanish Ministry of Science, Innovation and Universities and European Union NextGeneration-EU/PRTR (MCIN/AEI/10.13039/501100011033), through the Severo Ochoa FUNFUTURE (CEX2019-000917-S), PID2023-147211OB-C21, PDC2023-145874-I00, PID2020-116844RB-C21, PID2020-112548RB-I00, and PID2019-107727RB-I00 projects program, from Generalitat de Catalunya (2021 SGR 00804 and 2021 SGR 00651) and the European Research Council (2021-ERC-Advanced 'REMINDS' Grant No. 101054687) is acknowledged. We also acknowledge projects TED2021-130453B-C21 and TED2021-130453B-C22, funded by MCIN/AEI/10.13039/50110001103. This work was supported by: (i) the Portuguese Foundation for Science and Technology (FCT) in the framework of the Strategic Funding Contract UIDB/04650/2020; (ii) the exploratory research project 2022.01740.PDTC (**https://doi.org/10.54499/2022.01740.PTDC**) and (iii) the project M-ERA-NET3/0003/2021 – NanOx4EStor grant agreement No 958174 (**https://doi.org/10.54499/M-ERA-NET3/0003/2021**). J. P. B. S. also thanks FCT for the contract under the Institutional Call to Scientific Employment Stimulus – 2021 Call (CEECINST/00018/2021). This work was developed within the scope of the project CICECO-Aveiro Institute of Materials, UIDB/50011/2020, UIDP/50011/2020 & LA/P/0006/2020, financed by national funds through the FCT/MCTES (PIDDAC). Guillaume Sauthier from ICN2 is aknowledged for assistance on the XPS characterization. Francisco Javier Campos López is aknowledged for assistance on the X-ray characterization.

References

1 U. Schroeder, M. H. Park, T. Mikolajick and C. S. Hwang, *Nat. Rev. Mater.*, 2022, **7**, 653–669.
2 M. H. Park, D. Kwon, U. Schroeder and T. Mikolajick, *MRS Bull.*, 2021, **46**, 1071.
3 T. Schenk, M. Pesic, S. Slesazeck, U. Schroeder and T. Mikolajick, *Rep. Prog. Phys.*, 2020, **83**, 086501.
4 M. H. Park, D. H. Lee, K. Yang, J.-Y. Park, G. T. Yu, H. W. Park, M. Materano, T. Mittmann, P. D. Lomenzo, T. Mikolajick, U. Schroeder and C. S. Hwang, *J. Mater. Chem. C*, 2020, **8**, 10526–10550.
5 H. Chen, X. Zhou, L. Tang, Y. Chen, H. Luo, X. Yuan, C. R. Bowen and D. Zhang, *Appl. Phys. Rev.*, 2022, **9**, 011307.
6 J. Müller, T. S. Böscke, U. Schröder, S. Mueller, D. Bräuhaus, U. Böttger, L. Frey and T. Mikolajick, *Nano Lett.*, 2012, **12**, 4318–4323.
7 M. Yadav, A. Kashir, S. Oh, R. D. Nikam, H. Kim, H. Jang and H. Hwang, *Nanotechnology*, 2022, **33**, 085206.
8 K. Mizutani, T. Hoshii, H. Wakabayashi, K. Tsutsui, E. Y. Chang and K. Kakushima, *Jpn. J. Appl. Phys.*, 2022, **61**, 021006.
9 Y. Goh, S. H. Cho, S.-H. K. Park and S. Jeon, *Nanoscale*, 2020, **12**, 9024–9031.
10 J. Wang, D. Wang, Q. Li, A. Zhang, D. Gao, M. Guo, J. Feng, Z. Fan, D. Chen, M. Qin, M. Zeng, X. Gao, G. Zhou, X. Lu and J. M. Liu, *IEEE Electron Device Lett.*, 2019, **40**, 1937–1940.
11 H. A. Hsain, Y. Lee, S. Lancaster, P. D. Lomenzo, B. Xu, T. Mikolajick, U. Schroeder, G. N. Parsons and J. L. Jones, *Nanotechnology*, 2023, **34**, 125703.
12 B. Liu, Y. Cao, W. Zhang and Y. Li, *Appl. Phys. Lett.*, 2021, **119**, 172902.
13 T. Onaya, T. Nabatame, M. Inoue, T. Sawada, H. Ota and Y. Morita, *APL Mater.*, 2022, **10**, 051110.
14 N. A. Spaldin and R. Ramesh, *Nat. Mater.*, 2019, **18**, 203–212.
15 S. Manipatruni, D. E. Nikonov, C.-C. Lin, T. A. Gosavi, H. Liu, B. Prasad, Y.-L. Huang, E. Bonturim, R. Ramesh and I. A. Young, *Nature*, 2019, **565**, 35–42.

16 R. Thomas, J. F. Scott, D. N. Bose and R. S. Katiyar, *J. Phys.: Condens. Matter*, 2010, **22**, 423201.
17 C.-W. Nan, M. I. Bichurin, S. Dong, D. Viehland and G. Srinivasan, *J. Appl. Phys.*, 2008, **103**, 031101.
18 Y. Wang, J. Hu, Y. Lin and C.-W. Nan, *NPG Asia Mater.*, 2010, **2**, 61–68.
19 C. A. F. Vaz, J. Hoffman, C. H. Ahn and R. Ramesh, *Adv. Mater.*, 2012, **22**, 2900–2918.
20 C. Navarro-Senent, A. Quintana, E. Menéndez, E. Pellicer and J. Sort, *APL Mater.*, 2019, **7**, 030701.
21 A. Molinari, H. Hahn and R. Kruk, *Adv. Mater.*, 2019, **31**, 1806662.
22 Y. Guan, H. Han, F. Li, G. Li and S. S. P. Parkin, *Annu. Rev. Mater. Res.*, 2023, **53**, 25–51.
23 C. Binek and B. Doudin, *J. Phys.: Condens. Matter*, 2005, **17**, L39–L44.
24 S. Kopyl, R. Surmenev, M. Surmeneva, Y. Fetisov and A. Kholkin, *Mater. Today Bio*, 2021, **12**, 100149.
25 G. Srinivasan, E. Rasmussen, B. Levin and R. Hayes, *Phys. Rev. B*, 2002, **65**, 134402.
26 Y. Ma, W. Cheng, M. Ning and C. Ong, *Appl. Phys. Lett.*, 2007, **90**, 152911.
27 X. Lu, Y. Kim, S. Goetze, X. Li, S. Dong, P. Werner, M. Alexe and D. Hesse, *Nano Lett.*, 2011, **11**, 3202–3206.
28 I. Fina, N. Dix, J. M. Rebled, P. Gemeiner, X. Marti, F. Peiro, B. Dkhil, F. Sanchez, L. Fabrega and J. Fontcuberta, *Nanoscale*, 2013, **5**, 8037–8044.
29 A. Nicolenco, A. Gómez, X.-Z. Chen, E. Menéndez, J. Fornell, S. Pané, E. Pellicer and J. Sort, *Appl. Mater. Today*, 2020, **19**, 100579.
30 A. Dmitriyeva, V. Mikheev, S. Zarubin, A. Chouprik, G. Vinai, V. Polewczyk, P. Torelli, Y. Matveyev, C. Schlueter, I. Karateev, Q. Yang, Z. Chen, L. Tao, E. Y. Tsymbal and A. Zenkevich, *ACS Nano*, 2021, **15**, 14891–14902.
31 B. Vermeulen, F. Ciubotaru, M. I. Popovici, J. Swerts, S. Couet, I. P. Radu, A. Stancu, K. Temst, G. Groeseneken and C. Adelmann, *ACS Appl. Mater. Interfaces*, 2019, **11**, 34385–34393.
32 S. Lancaster, I. Arnay, R. Guerrero, A. Gudín, A. Guedeja-Marrón, J. M. Diez, J. Gärtner, A. Anadón, M. Varela, J. Camarero, T. Mikolajick, P. Perna and S. Slesazeck, *ACS Appl. Mater. Interfaces*, 2023, **15**, 16963–16974.
33 Y. Wei, P. Nukala, M. Salverda, S. Matzen, H. J. Zhao, J. Momand, A. Everhardt, G. R. Blake, P. Lecoeur and B. J. Kooi, *Nat. Mater.*, 2018, **17**, 1095.
34 J. Lyu, I. Fina, R. Solanas, J. Fontcuberta and F. Sánchez, *Appl. Phys. Lett.*, 2018, **113**, 082902.
35 Y. Wei, S. Matzen, C. P. Quinteros, T. Maroutian, G. Agnus, P. Lecoeur and B. Noheda, *npj Quantum Mater.*, 2019, **4**, 1–6.
36 Y. Wei, S. Matzen, T. Maroutian, G. Agnus, M. Salverda, P. Nukala, Q. Chen, J. Ye, P. Lecoeur and B. Noheda, *Phys. Rev. Appl.*, 2019, **12**, 031001.
37 J. Lyu, I. Fina, J. Fontcuberta and F. Sánchez, *ACS Appl. Mater. Interfaces*, 2019, **11**, 6224–6229.
38 R. Meyer, R. Waser, K. Prume, T. Schmitz and S. Tiedke, *Appl. Phys. Lett.*, 2005, **86**, 142907.
39 I. Fina, L. Fabrega, E. Langenberg, X. Marti, F. Sánchez, M. Varela and J. Fontcuberta, *J. Appl. Phys.*, 2011, **109**, 074105.
40 G. Kresse and J. Furthmüller, *Comput. Mater. Sci.*, 1996, **6**, 15–50.
41 G. Kresse and J. Furthmüller, *Phys. Rev. B: Condens. Matter Mater. Phys.*, 1996, **54**, 11169–11186.
42 J. P. Perdew, A. Ruzsinszky, G. I. Csonka, O. A. Vydrov, G. E. Scuseria, L. A. Constantin, X. Zhou and K. Burke, *Phys. Rev. Lett.*, 2008, **100**, 136406.
43 G. Kresse and D. Joubert, *Phys. Rev. B: Condens. Matter Mater. Phys.*, 1999, **59**, 1758–1775.
44 A. van de Walle, P. Tiwary, M. de Jong, D. L. Olmsted, M. Asta, A. Dick, D. Shin, Y. Wang, L. Q. Chen and Z. K. Liu, *Calphad*, 2013, **42**, 13–18.
45 R. Resta and Rev Mod, *Phys.*, 1994, **66**, 899–915.
46 M. Gajdoš, K. Hummer, G. Kresse, J. Furthmüller and F. Bechstedt, *Phys. Rev. B*, 2006, **73**, 045112.
47 A. G. Chernikova and A. M. Markeev, *Appl. Phys. Lett.*, 2021, **119**, 032904.
48 E. Goyat, S. Hait, V. Barwal, G. Goyat, R. Siwach and S. Chaudhary, *J. Supercond. Novel Magn*, 2022, **35**, 2029–2036.
49 J. Nogués, J. Sort, V. Langlais, V. Skumryev, S. Suriñach, J. S. Muñoz and M. D. Baró, *Phys. Rep.*, 2005, **422**, 65–117.
50 G. Catalan, *Appl. Phys. Lett.*, 2006, **88**, 102902.
51 W. Brown, *Handbook of Chemistry and Physics*, McGraw-Hill, New York, New York City, 1958.
52 B. C. Jeon, D. Lee, M. H. Lee, S. M. Yang, S. C. Chae, T. K. Song, S. D. Bu, J.-S. Chung, J.-G. Yoon and T. W. Noh, *Adv. Mater.*, 2013, **25**, 5643–5649.
53 H. Lu, C.-W. Bark, D. Esque de los Ojos, J. Alcala, C. B. Eom, G. Catalan and A. Gruverman, *Science*, 2012, **336**, 59–61.
54 D. Lee, S. M. Yang, J.-G. Yoon and T. W. Noh, *Nano Lett.*, 2012, **12**, 6436–6440.
55 W. Ma, *Phys. Status Solidi B*, 2008, **245**, 761–768.
56 A. K. Jena, A. K. Sahoo and J. Mohanty, *Appl. Phys. Lett.*, 2020, **116**, 092901.
57 B. Sun, Y. Liu, W. Zhao and P. Chen, *RSC Adv.*, 2015, **5**, 13513–13518.
58 M. D. Glinchuk, A. N. Morozovska, A. Lukowiak, W. Stręk, M. V. Silibin, D. V. Karpinsky, Y. Kim and S. V. Kalinin, *J. Alloys Compd.*, 2020, **830**, 153628.
59 P. Nukala, M. Ahmadi, Y. Wei, S. De Graaf, E. Stylianidis, T. Chakrabortty, S. Matzen, H. W. Zandbergen, A. Björling and D. Mannix, *Science*, 2021, **372**, 630–635.
60 T. Song, F. Sánchez and I. Fina, *APL Mater.*, 2022, **10**, 031108.
61 M. G. Kozodaev, A. G. Chernikova, E. V. Korostylev, M. H. Park, R. R. Khakimov, C. S. Hwang and A. M. Markeev, *J. Appl. Phys.*, 2019, **125**, 034101.

